Acta Crystallographica Section D
Biological Crystallography
ISSN 1399-0047

Structure of choline oxidase in complex with the reaction product glycine betaine

Francesca Salvi,[a] Yuan-Fang Wang,[b] Irene T. Weber[a,b,c,d]* and Giovanni Gadda[a,b,c,d]*

[a]Department of Chemistry, Georgia State University, PO Box 3965, Atlanta, GA 30302-3965, USA, [b]Department of Biology, Georgia State University, PO Box 4010, Atlanta, GA 30302-4010, USA, [c]Center for Biotechnology and Drug Design, Georgia State University, Atlanta, Georgia, USA, and [d]Center for Diagnostics and Therapeutics, Georgia State University, Atlanta, Georgia, USA

Correspondence e-mail: iweber@gsu.edu, ggadda@gsu.edu

Received 9 September 2013
Accepted 23 October 2013

PDB reference: choline oxidase, complex with glycine betaine, 4mjw

Choline oxidase from *Arthrobacter globiformis*, which is involved in the biosynthesis of glycine betaine from choline, has been extensively characterized in its mechanistic and structural properties. Despite the knowledge gained on the enzyme, the details of substrate access to the active site are not fully understood. The 'loop-and-lid' mechanism described for the glucose–methanol–choline enzyme superfamily has not been confirmed for choline oxidase. Instead, a hydrophobic cluster on the solvent-accessible surface of the enzyme has been proposed by molecular dynamics to control substrate access to the active site. Here, the crystal structure of the enzyme was solved in complex with glycine betaine at pH 6.0 at 1.95 Å resolution, allowing a structural description of the ligand–enzyme interactions in the active site. This structure is the first of choline oxidase in complex with a physiologically relevant ligand. The protein structures with and without ligand are virtually identical, with the exception of a loop at the dimer interface, which assumes two distinct conformations. The different conformations of loop 250–255 define different accessibilities of the proposed active-site entrance delimited by the hydrophobic cluster on the other subunit of the dimer, suggesting a role in regulating substrate access to the active site.

1. Introduction

Choline oxidase (EC 1.1.3.17) from *Arthrobacter globiformis* catalyzes the oxidation of choline to glycine betaine (Fig. 1), which is a ubiquitous osmoprotectant in bacteria, plants and animals (Bremer & Kramer, 2000). The enzyme is important in biotechnological applications for the genetic engineering of economically relevant plants to potentiate osmotic stress resistance (Sakamoto & Murata, 2000; Giri, 2011) and the development of sensors for the detection of choline and derivatives in biological fluids (Shimomura *et al.*, 2009). The oxidation of choline to glycine betaine catalyzed by choline oxidase occurs *via* two hydride-transfer reactions, with the rate-limiting steps represented by the two flavin reductions (Fig. 1; Fan & Gadda, 2005*a*). Studies of the temperature dependence of the substrate kinetic isotope effect in choline oxidase demonstrated that the hydride transfer in alcohol oxidation occurs quantum-mechanically within a pre-organized enzyme–substrate complex (Fan & Gadda, 2005*b*). The reaction intermediate betaine aldehyde has been shown to predominantly exist in the *gem*-diol form in solution (Fan *et al.*, 2006) and to stay bound in the active site of the enzyme in bacteria (Fig. 1; Gadda, 2003). In fungi, it is instead released

to bulk solvent when the enzyme turns over with choline (Lambou *et al.*, 2013). Choline oxidase contains FAD covalently linked to the protein through His99 (Quaye *et al.*, 2009). The enzyme is grouped into the glucose–methanol–choline (GMC) enzyme oxidoreductase superfamily (Cavener, 1992), which includes a variety of FAD-dependent enzymes that oxidize unrelated alcohols and share similar three-dimensional structures (Salvi & Gadda, 2013). The mechanism of action of bacterial choline oxidase has been extensively characterized (Quaye *et al.*, 2008), with structural and mechanistic studies showing the importance of residues Ser101 (Yuan & Gadda, 2011), Glu312 (Quaye *et al.*, 2008), His351 (Rungsrisuriyachai & Gadda, 2008), Val464 (Finnegan, Agniswamy *et al.*, 2010; Gadda, 2012*a*), His466 (Ghanem & Gadda, 2005) and Asn510 (Rungsrisuriyachai & Gadda, 2010) in the active site.

The crystallographic structure of wild-type choline oxidase has previously been reported (PDB entry 2jbv) from single crystals obtained at pH 8.5 (Quaye *et al.*, 2008). It shows a distorted flavin with an O atom covalently linked to the flavin C(4a) atom of the isoalloxazine ring and contains DMSO from the crystallization cocktail in the active site (Quaye *et al.*, 2008). Two crystal structures of active-site mutants are also available from crystallization conditions at pH 6.0, *i.e.* the S101A enzyme in complex with acetate (PDB entry 3nne; Finnegan, Yuan *et al.*, 2010) and the V464A enzyme devoid of ligands (PDB entry 3ljp; Finnegan, Agniswamy *et al.*, 2010). In all cases the enzyme crystallizes as a dimer, and biochemical studies established a dimeric state for the enzyme in solution (Fan *et al.*, 2004). The enzyme active site is completely secluded from bulk solvent (Quaye *et al.*, 2008; Finnegan, Yuan *et al.*, 2010), raising the question of how the substrate accesses the active site. A 'loop-and-lid' mechanism has been proposed to control substrate access in the homotetrameric pyranose 2-oxidase (Bannwarth *et al.*, 2004; Spadiut *et al.*, 2010; Hallberg *et al.*, 2004; Kujawa *et al.*, 2006) and monomeric cholesterol oxidase (Yue *et al.*, 1999; Chen *et al.*, 2000; Sampson *et al.*, 1998), which are members of the GMC enzyme superfamily. The corresponding loop that covers the active site in choline oxidase (*e.g.* residues 74–85) is well defined in the available crystal structures and it was shown to be static over 60 ns in molecular-dynamics simulations (Xin *et al.*, 2009). In contrast, rapid dynamic motions of a hydrophobic cluster composed of Met62, Lys65, Val355, Phe357 and Met359 on the solvent-accessible surface above the FAD cofactor were observed (Xin *et al.*, 2009). The side chains of these residues delimit the entrance of a tunnel leading to the active site (Fig. 2) and their motions regulate the radius of this entrance.

In this study, we report the three-dimensional structure of choline oxidase in complex with glycine betaine solved to 1.95 Å resolution, allowing the description of key interactions of active-site residues with the reaction product of choline oxidation. The FAD cofactor is not modified on its C(4a) atom, as in the published structure of the wild-type enzyme (Quaye *et al.*, 2008). The dimer structure of the enzyme in its complexes with glycine betaine and DMSO showed different conformations of a solvent-accessible loop covering the hydrophobic cluster of the other subunit, underlying the importance of the dimeric state of the enzyme for catalysis.

2. Experimental procedures

2.1. Materials

Escherichia coli strain Rosetta(DE3)pLysS was obtained from Novagen (Madison, Wisconsin, USA). Magnesium acetate and PEG 6000 were purchased from Sigma–Aldrich (St Louis, Missouri, USA), calcium chloride and choline chloride were from ICN Biomedicals (Irvine, California, USA) and glycerol was from Thermo Fisher Scientific (Waltham, Massachusetts, USA). All other reagents were of the highest purity commercially available.

2.2. Crystallization and X-ray data collection

Recombinant choline oxidase from *A. globiformis* was expressed in *E. coli* strain Rosetta(DE3)pLysS and purified as described previously (Fan *et al.*, 2004). The protein was stored in 20 m*M* Tris–HCl pH 8.0. A single crystal was grown by the

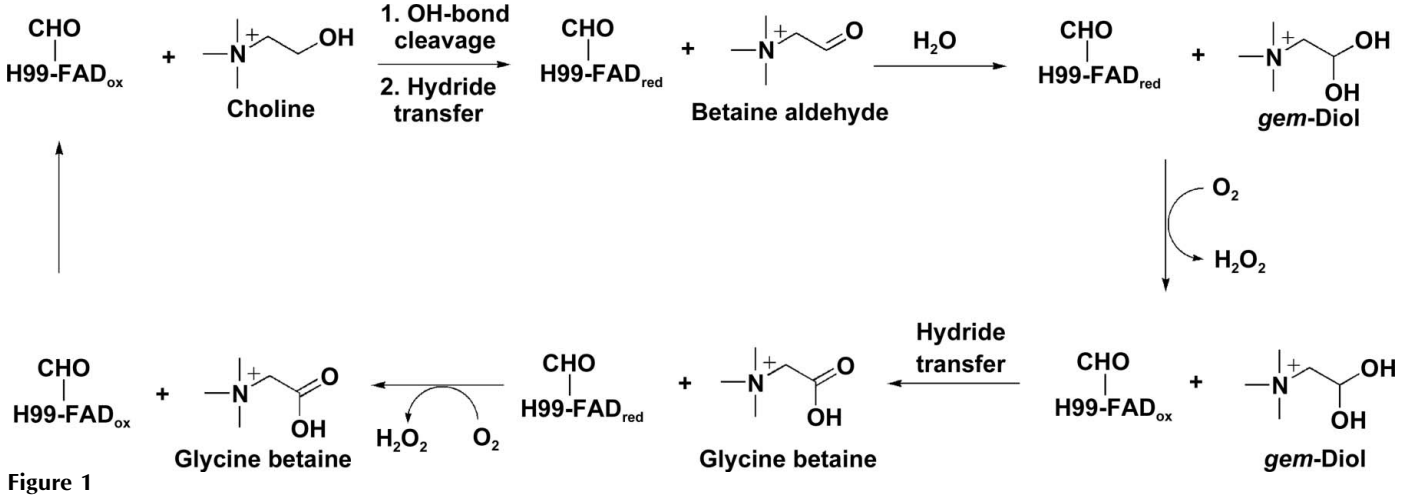

Figure 1
The oxidation of choline to glycine betaine by choline oxidase.

hanging-drop vapor-diffusion method at room temperature by mixing 1 µl choline oxidase (6.6 mg ml^{-1}) with 1 µl reservoir solution consisting of 0.1 *M* magnesium acetate pH 6.0, 50 m*M* calcium chloride, 2.5%(*v*/*v*) glycerol, 10%(*w*/*v*) PEG 6000. The enzyme drop was equilibrated against 500 µl reservoir solution and crystal growth was observed in 1 d. The crystal was soaked in reservoir solution with 1 *M* choline chloride and 20% glycerol as a cryoprotectant for ∼1 min and cooled immediately in liquid nitrogen. X-ray data were collected at 100 K on beamline 22-ID of the Southeast Regional Collaborative Access Team (SER-CAT) at the Advanced Photon Source, Argonne National Laboratory.

2.3. Structure determination and model refinement

The X-ray data were integrated and scaled using *HKL*-2000 (Otwinowski & Minor, 1997). The structure was solved by molecular replacement using *Phaser* (McCoy *et al.*, 2005) in the *CCP*4 suite of programs (Winn *et al.*, 2011) using the previously published crystal structure of choline oxidase as the initial model (PDB entry 2jbv; Quaye *et al.*, 2008). The crystal structure was refined with *REFMAC* (Murshudov *et al.*, 2011) and manual adjustment and rebuilding were performed using *Coot* (Emsley & Cowtan, 2004). In both subunits glycine betaine was refined with 0.5 occupancy as suggested by the weak electron density. Higher peaks in the electron-density map were observed for the two O atoms of the carboxylate group, while lower density peaks were observed for the other atoms. The crystal structure was deposited as PDB entry 4mjw.

Protein structures were superimposed on C$^{\alpha}$ atoms using *SUPERPOSE* from the *CCP*4 suite (Krissinel & Henrick, 2004). Structural figures were generated with *PyMOL* (http://www.pymol.org) and *CCP*4*mg* (McNicholas *et al.*, 2011). The detection of tunnels to the active site was performed with *CAVER* (Chovancova *et al.*, 2012). The number of approximating balls was set at 12, the minimum probe radius was 1.0 Å, the shell depth was 4 Å, the shell radius was 3 Å, the clustering threshold was 3.5 and the starting point was set to the N(5) atom of the flavin cofactor with a maximum distance of 3 Å and a desired radius of 5 Å.

3. Results

3.1. Structure of choline oxidase in complex with glycine betaine

The structure of choline oxidase in complex with the reaction product glycine betaine at pH 6.0 was solved in space group $P4_32_12$ after soaking the protein crystals in a solution with 1 *M* choline chloride. The space group was the same as previously seen for the structures at pH 8.5 of the enzyme co-crystallized with DMSO bound at the active site (PDB entry 2jbv; Quaye *et al.*, 2008) and the active-site variant V464A devoid of ligands at pH 6.0 (PDB entry 3ljp; Finnegan, Agniswamy *et al.*, 2010). The structure was refined to an *R* factor of 0.15 and a resolution of 1.95 Å. The crystallographic data and refinement statistics are presented in Table 1.

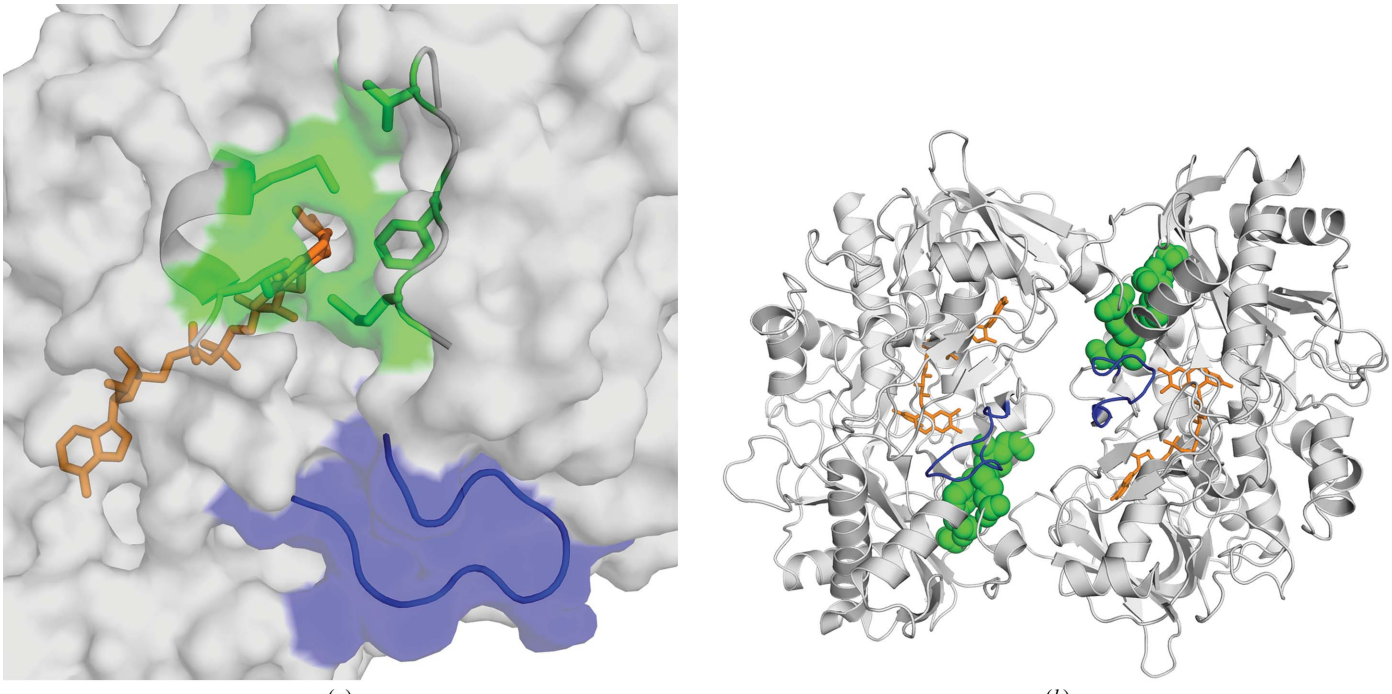

(*a*) (*b*)

Figure 2
The hydrophobic cluster on the solvent-accessible surface of choline oxidase. (*a*) The surface of wild-type choline oxidase in complex with DMSO (PDB entry 2jbv) is shown in light gray, the side chains of the hydrophobic cluster Met62, Leu65, Val355, Phe357 and Met359 are shown as green sticks, loop 74–85 is highlighted in blue and FAD is shown as orange sticks. (*b*) The positions of the hydrophobic cluster and of loop 74–85 at the dimer interface are shown in the dimer structure. The backbone structure of the dimeric enzyme is shown in light gray, the hydrophobic cluster is shown as green spheres, FAD is shown in orange sticks and loop 74–85 is colored blue.

The enzyme–product complex crystallized as a homodimer, with each monomer consisting of FAD-binding and substrate-binding domains. Overall, the fold of the protein polypeptide was the same as those previously described for choline oxidase in complex with DMSO (Quaye *et al.*, 2008) and two active-site variants, *i.e.* the S101A enzyme in complex with acetate (Finnegan, Yuan *et al.*, 2010) and the V464A enzyme devoid of ligands (Finnegan, Agniswamy *et al.*, 2010). Superimposition of the C^{α} atoms of the enzyme in its complexes with glycine betaine and DMSO yielded r.m.s.d. values of 0.50 and 0.48 Å for the *A* and *B* chains over 526 and 529 amino-acid residues, respectively, indicating that the two structures were practically identical. Most of the symmetrical hydrogen-bonding and electrostatic interactions between the two monomers in each dimeric structure that were previously described in the DMSO complex structure (Quaye *et al.*, 2008) are maintained in the enzyme–glycine betaine structure. The main interactions at the dimer interface are two symmetric sets of ionic pairs (with distance ranges listed in parentheses), Asp358–Arg396 (2.9–3.1 Å) in subunit *A* and Arg363–Asp397 (2.8–3.0 Å) in subunit *B*, and one symmetric set of hydrogen bonds, Thr256–Glu370 (2.8 Å in subunit *A* and 2.9 Å in subunit *B*). The nonpolar interactions of Phe253 with residues in the other subunit differ in the complexes with glycine betaine and DMSO (see below).

Table 1
X-ray diffraction data-collection and model-refinement statistics.

Values in parentheses are for the highest resolution shell.

Data collection	
Space group	$P4_32_12$
Unit-cell parameters (Å)	a = 87.4, c = 353.5
Wavelength (Å)	0.8
Resolution (Å)	43.4–1.95 (2.02–1.95)
No. of reflections (total)	1072541
No. of reflections (unique)	97679 (8823)
R_{merge} (%)	9.8 (42.8)
$\langle I/\sigma(I)\rangle$	14.2 (3.0)
Completeness (%)	97.0 (89.3)
Multiplicity	4.5 (3.6)
$CC_{1/2}$	0.863
Refinement	
R_{work}/R_{free} (%)	15.3/18.1
No. of atoms	
Protein	8214
Ligand (FAD, BET)	122
Solvent	766
Isotropic B factors (Å^2)	
Protein (main chain)	12.4
Protein (side chain)	16.3
FAD	11.1
Glycine betaine	22.9
Solvent molecules	25.3
R.m.s. deviations	
Bonds length (Å)	0.016
Angle distance (Å)	2.3
Ramachandran plot statistics	
Residues in favored region	1026 [96.9%]
Residues in allowed region	32 [3.0%]
Residues in non-allowed region	1 [0.1%]

3.2. FAD-binding site

The electron-density map of the FAD cofactor is well defined and clearly indicates the covalent linkage to His99. FAD is buried in the flavin-binding domain and occupies the same position previously established in other crystal structures of the enzyme. A notable difference between the structures of the wild-type enzyme is that the isoalloxazine in the structure presented here does not contain an O atom covalently linked to the C(4a) atom, as previously reported for the enzyme in complex with DMSO (Fig. 3; Quaye *et al.*, 2008; Orville *et al.*, 2009). Consequently, the conformation of the isoalloxazine in the glycine betaine complex is fairly planar, with a slight V-shaped bend on the N(5)–N(10) axis. This is consistent with the flavin being in the reduced state, as observed for a number of other flavoenzymes (Fu *et al.*, 2010; Dixon *et al.*, 1979), in agreement with the result that although choline was added to the protein crystal the product of its oxidation is found in the active site of the enzyme. The reduced state of the FAD

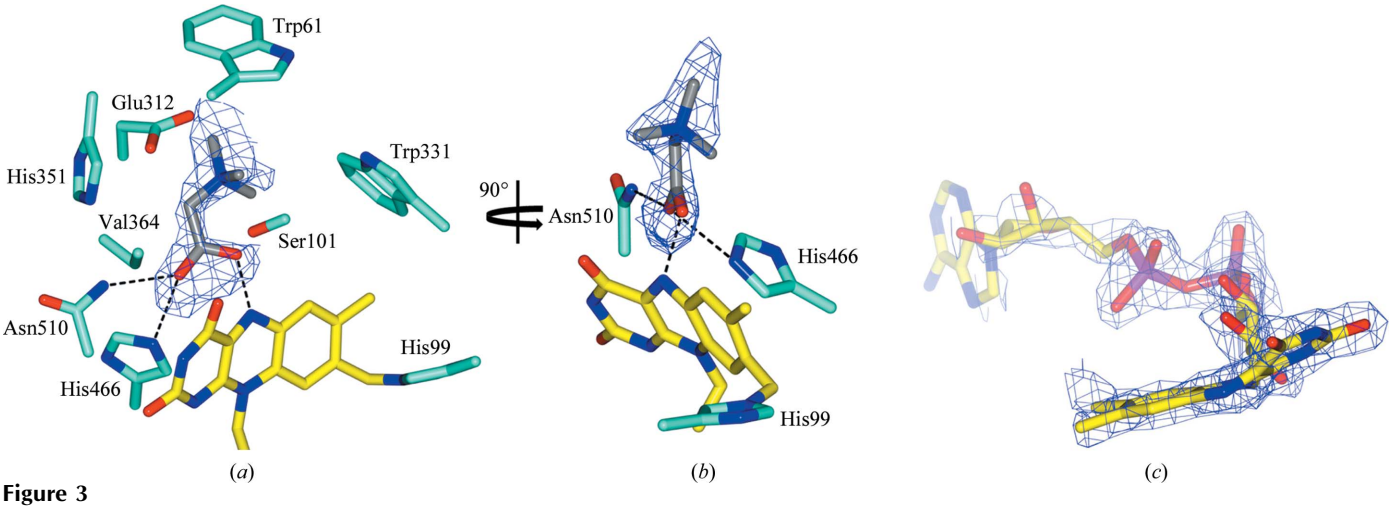

Figure 3
Interactions of glycine betaine in the active site of choline oxidase and the conformation of the FAD cofactor in the structure of choline oxidase presented in this study. (*a*, *b*) Glycine betaine in subunit *B* is shown as gray sticks, the OMIT map contoured at 0.4 e Å^{-3} is shown in blue, FAD is shown as yellow sticks. The side chains of the residues close to glycine betaine are displayed as cyan sticks and labeled; hydrogen bonds are highlighted with black dashes. For clarity Tyr465 is not shown. (*c*) FAD is shown as yellow sticks and the electron-density map ($2F_o - F_c$) contoured at 0.7 e Å^{-3} is shown in blue.

cofactor is further confirmed by the change in color of the crystal from yellow to colorless that was observed on exposure to X-rays.

3.3. Glycine betaine binding

After refinement of the atoms belonging to the protein, FAD cofactor and waters, electron density not consistent with water molecules in shape and distance was present in front of the *re* face of the isoalloxazine ring. This electron density was tentatively modeled with various components of the crystallization cocktail, the substrate choline, the reaction product glycine betaine or the reaction intermediate betaine aldehyde. The product glycine betaine gave the best fit to the electron density (Fig. 3). The carboxylate O atoms were a good fit to the electron density near the flavin, while choline has only a single hydroxyl group in the corresponding position. The planar carboxylate group of glycine betaine also was a good fit to the electron density that is consistent with the sp^2 character of the carboxylate C atom. This part of the electron density could not be modeled with an sp^3-hybridized C atom as present in choline. The presence of the product glycine betaine in the active site rather than choline is also in agreement with the notion that the reaction with choline is fast (Fan & Gadda, 2005*a*) and that product release would be more difficult in the crystal.

The interactions of glycine betaine in the active site of choline oxidase are shown in Fig. 3. The closest contact between the ligand and the flavin is through an O atom of the carboxylate of glycine betaine, which is at a distance of 2.7 Å in subunit *A* and 2.6 Å in subunit *B* from the N(5) atom of FAD. Other interactions of the ligand carboxylate are with the O(4) atom of FAD (3.4 Å in subunit *A* and 3.3 Å in subunit *B*), the side-chain amide of Asn510 (2.8 and 3.0 Å in subunits *A* and *B*, respectively) and the $N^{\varepsilon 2}$ atom of His466 (3.1 and 3.3 Å). Further contacts of the ligand carboxylate are with the hydroxyl of Ser101 (3.3 and 3.6 Å). The C^{α} atom of glycine betaine is close to the side chains of Val464 (3.4 and 3.6 Å) and His351 (3.3 and 3.6 Å). The positively charged trimethylammonium moiety of glycine betaine is proximal to the aromatic side chains of Trp61 (4.0 and 3.9 Å), Trp331 (3.9 and 3.6 Å) and Tyr465 (3.9 and 4.1 Å). The trimethylammonium group of glycine betaine is 4.0 and 3.8 Å away from the carboxylate of the side chain of Glu312 in subunits *A* and *B*, respectively.

3.3.1. Conformations of the loop comprising residues 250–255. As illustrated in Fig. 4, the superimposition of the structures of choline oxidase in complex with glycine betaine and DMSO showed two different conformations of loop 250–255 at the dimer interface in both subunits of the dimer. The two conformations of loop 250–255 are significantly different, with a largest distance between the C^{α} atoms of residue Ala252 of 7.5 Å in subunit *A* and 7.7 Å in subunit *B* in the two

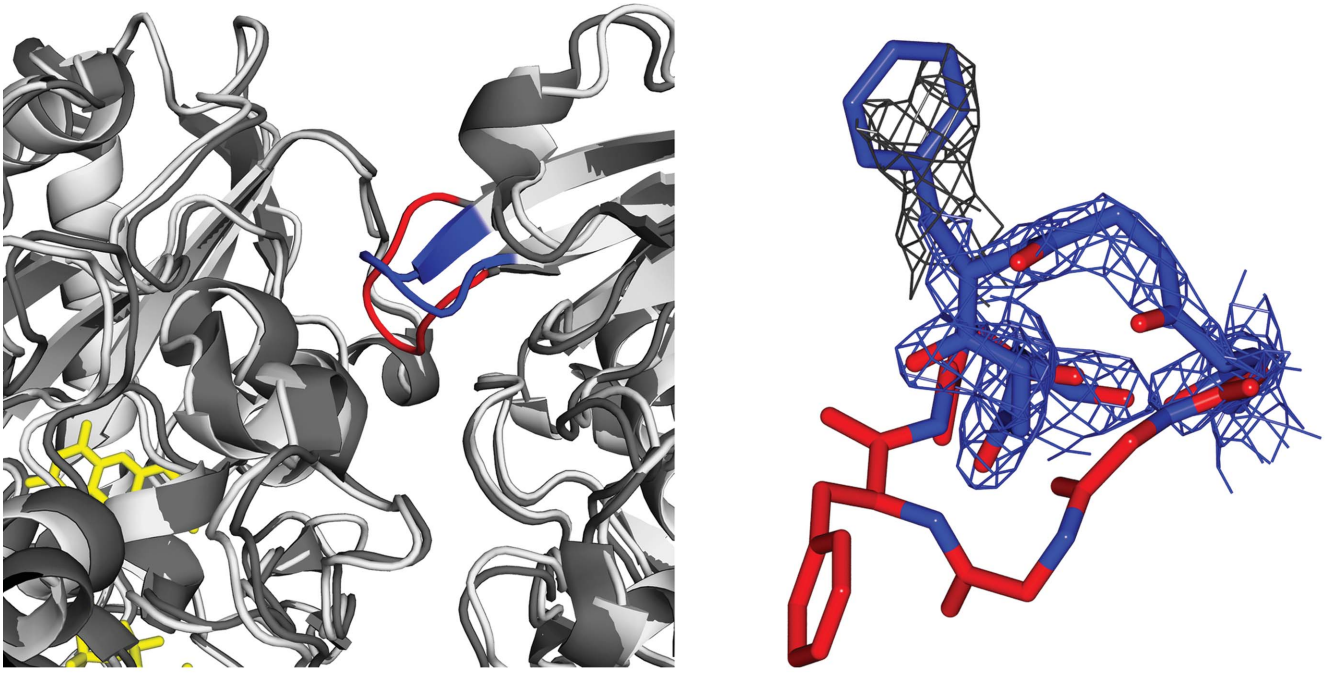

(*a*) (*b*)

Figure 4
Different conformations of loop 250–255 in the crystal structures of choline oxidase in complex with glycine betaine and with DMSO (PDB entry 2jbv). (*a*) The superimposed structures are shown as a light gray cartoon for choline oxidase in complex with glycine betaine and as a dark gray cartoon for choline oxidase in complex with DMSO (PDB entry 2jbv). The FAD cofactor of choline oxidase in complex with glycine betaine is shown in yellow sticks; the conformations of the main chains of loop 250–255 are highlighted in red for choline oxidase in complex with DMSO (PDB entry 2jbv) and in blue for choline oxidase in complex with glycine betaine. For clarity, only loop 250–255 of subunit *B* is shown. (*b*) The main chain of the residues of loop 250–255 and the side chain of Phe253 of choline oxidase with glycine betaine are shown as blue sticks and the electron density of the OMIT map is shown in blue (contoured at 0.5 e $Å^{-3}$) and in gray (contoured at 0.33 e $Å^{-3}$); the same atoms in the structure with DMSO (PDB entry 2jbv) are shown as red sticks.

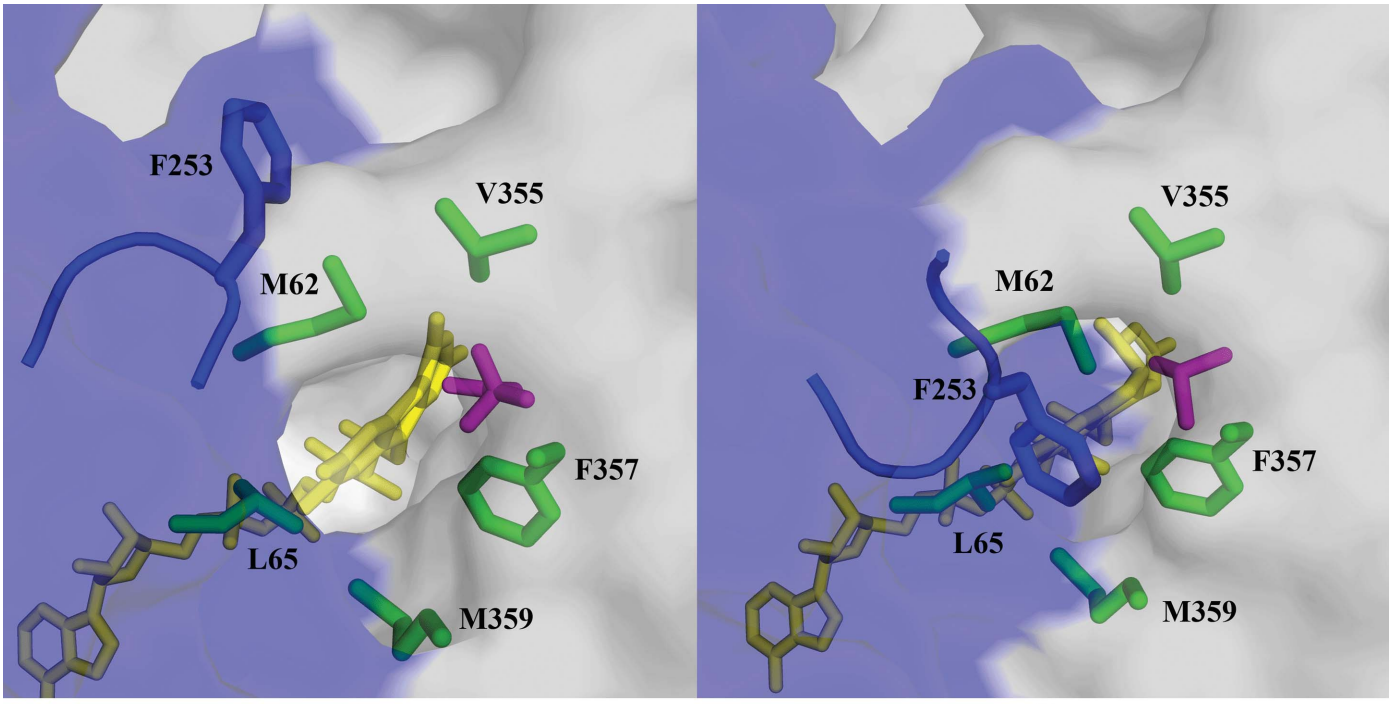

Figure 5
Positions of Phe253 in the open and closed conformations of loop 250–255. The side chains of the hydrophobic cluster Met62, Leu65, Val355, Phe357 and Met359 of chain *A* are shown as green sticks, while Phe253 of chain *B* is shown as blue sticks. FAD is shown as yellow sticks and the flavin rings are accessible from the surface through the tunnel to the active site. The surface is shown in gray in subunit *A* and in blue in subunit *B*. (*a*) Choline oxidase in complex with glycine betaine (open conformation) is shown in surface representation with glycine betaine as magenta sticks. (*b*) Choline oxidase in complex with DMSO (closed conformation) is shown as a gray surface and DMSO is shown as magenta sticks.

superimposed structures. In the structure of the enzyme–glycine betaine complex, the side chain of Phe253 is partially disordered beyond C^{γ} with atoms visible in the electron density only at lower contour levels. Similar disorder of the Phe253 side chain is also observed in the enzyme–DMSO complex. The electron densities of the remaining portions of loop 250–255 are instead defined well in both complexes. By lowering the contour limits of the $2F_o - F_c$ electron-density maps to 0.5 e Å^{-3} (1.49 r.m.s.d.) and 0.33 e Å^{-3} (0.99 r.m.s.d.) for the enzyme–DMSO and the enzyme–glycine betaine complexes in Fig. 4(*b*) (the former is not shown for clarity), it is evident that the side chain of Phe253 points in different directions in the two structures (Fig. 5). In the complex with glycine betaine, the side chain of Phe253 is close to Tyr330 (3.5 and 3.6 Å in subunits *A* and *B*, respectively) of the other subunit. In the enzyme–DMSO complex, the aromatic ring of Phe253 instead stacks on the side chains of Met62 (4.0 and 4.2 Å), Leu65 (3.6 and 4.3 Å), Phe357 (4.7 and 3.6 Å) and Met359 (3.1 and 3.4 Å) of the other subunit. We define the conformation observed in the structure with glycine betaine in the active site as 'open', and the 'closed' conformation is seen in the previously published structure of the enzyme in complex with DMSO (PDB entry 2jbv; Quaye *et al.*, 2008). Analysis of the published structures of choline oxidase demonstrates that both open and closed conformations are present in the two subunits of the V464A enzyme dimer at pH 6.0 (PDB entry 3ljp; Finnegan, Agniswamy *et al.*, 2010), whereas the S101A enzyme (PDB entry 3nne; Finnegan, Yuan *et al.*, 2010) crystallized with acetate in the active site at pH 6.0 displays only the closed conformation in all eight subunits present in the crystallographic structure (data not shown).

3.3.2. Predicted tunnels to the active site. One tunnel with a radius of 1.0 Å was identified using *CAVER* that connects the surface of choline oxidase in complex with glycine betaine with the active site of the enzyme, as shown in Fig. 6. This tunnel is delimited by the side chains of the hydrophobic cluster Met62, Leu65, Val355, Phe357 and Met359, which was previously predicted to gate the access of the substrate to the active site through molecular dynamics (Baron *et al.*, 2009). In the structure of the wild-type enzyme in complex with DMSO no tunnel was predicted to pass through the hydrophobic cluster, primarily owing to steric hindrance by the side chain of Phe253 from the other subunit of the dimer (Fig. 6*b*). Thus, it appears that the conformation of the side chain of Phe253 from the other subunit of the dimeric structure determines whether the tunnel is open or closed.

4. Discussion

The present study reports the first crystal structure of choline oxidase in complex with glycine betaine, the product of the oxidation of choline catalyzed by the enzyme. Prior to this study, two other structures of choline oxidase in complex with components of the crystallization solution (DMSO or acetate) had been reported (Quaye *et al.*, 2008; Finnegan, Yuan *et al.*, 2010), but none with physiologically relevant molecules.

Within the GMC enzyme oxidoreductase superfamily, the structure of fungal pyranose 2-oxidase from *Peniophora* sp. is the only other example of an alcohol oxidase in complex with a reaction product, *i.e.* 2-keto-β-D-glucose (Bannwarth *et al.*, 2006). The structure of the choline oxidase–glycine betaine complex is therefore an important breakthrough that complements previous mechanistic investigations on the catalytic roles of several amino-acid residues in the active site of the enzyme (Quaye *et al.*, 2008, 2009, 2010; Rungsrisuriyachai & Gadda, 2008, 2010; Ghanem & Gadda, 2005; Yuan & Gadda, 2011; Finnegan, Yuan *et al.*, 2010; Gadda, 2012*b*; Finnegan, Agniswamy *et al.*, 2010; Quaye & Gadda, 2009; Finnegan & Gadda, 2008; Gadda *et al.*, 2006). The comparison of the structure of the enzyme–product complex reported here with those previously obtained for choline oxidase allowed the identification of conformational and topological differences at the dimer interface, with implications for the mechanism of substrate access to the active site. We assume that the conformational differences arise from the different crystallization conditions or the presence of mutations, since the compared crystal structures were refined in the same space group with similar unit-cell parameters; however, the crystal contacts are likely to constrain the enzyme dynamics.

The closest interaction of the carboxylate of glycine betaine with the flavin is with the N(5) atom of the isoalloxazine (Fig. 3). The carboxylate group also interacts with the protein through the side chains of His466 and Asn510 (Fig. 3). Despite its proximity, the carboxylate of glycine betaine is likely to not interact with the hydroxyl of Ser101 owing to a non-optimal orientation for hydrogen bonding. It is noteworthy to consider that the carboxylate C atom of glycine betaine is the same C atom that is oxidized in choline in the reaction catalyzed by choline oxidase, *i.e.* the C^{α} atom carrying the hydroxyl O atom and from which the hydride ion that reduces the flavin originates. Thus, all of the interactions between the carboxylate of glycine betaine in the active site are consistent with the mechanism for the oxidation of choline, in which (i) a hydride ion is transferred from the choline C^{α} atom to the flavin N(5) atom, as suggested by kinetic isotope effects (Fan & Gadda, 2005*a*,*b*, 2007), (ii) the serine hydroxyl stabilizes the transition state for the proton-transfer reaction that converts choline to choline alkoxide, as suggested by mutagenesis of Ser101 (Yuan & Gadda, 2011), (iii) the positively charged imidazolium of His466 stabilizes the alkoxide reaction intermediate in the oxidation of choline, as suggested by activity rescuing of the H466A mutant at low pH (Ghanem & Gadda, 2005), and (iv) Asn510 is important for the relative timing for the cleavage of the OH and CH bonds of choline, as suggested by multiple kinetic isotope effect studies of choline oxidase with Asn510 replaced with alanine or histidine (Rungsrisuriyachai & Gadda, 2010).

The position of His466 near the carboxylate of glycine betaine suggests that this residue may be the catalytic base that carries out substrate activation to the alkoxide species by catalyzing the cleavage of the alcohol OH bond. In this respect, the previous characterization of the mutant enzymes H466A (Ghanem & Gadda, 2005) or H351A (Rungsrisuriyachai & Gadda, 2008) showed that an active-site base was still present in the active sites of these enzymes, as suggested by the pH profiles of $k_{cat}/K_{choline}$ (Rungsrisuriyachai & Gadda, 2008; Ghanem & Gadda, 2005). However, a water molecule acting as surrogate base could occupy the space of the imidazole side chains of the histidine residues when they have been substituted with alanine in the mutant enzymes. This hypothesis is being currently investigated on a mutant choline oxidase in which His466 is replaced with glutamine. His466 is fully conserved in the active sites of the GMC enzymes, and its counterpart in pyranose 2-oxidase and aryl-alcohol oxidase has been shown to act as a base (Wongnate *et al.*, 2011; Hernández-Ortega *et al.*, 2011).

The trimethylammonium moiety of glycine betaine interacts with the side chains of Trp61, Tyr465 and Trp331 (Fig. 3). The trimethylammonium group is preserved in the oxidation of choline to glycine betaine; therefore, similar interactions with the enzyme are expected for this group in the product and substrate complexes. The trimethylammonium group is also at a distance of 4.0 and 3.6 Å in subunits *A* and *B*, respectively, from the side chain of Glu312. The importance of Glu for substrate binding has been established through mechanistic studies of the enzyme variant E312Q, which showed a 500-fold increase in the K_d value for choline in rapid kinetics (Quaye *et al.*, 2008). An independent mechanistic study with choline analogs carrying one or two methyls on the amine portion of the molecule demonstrated

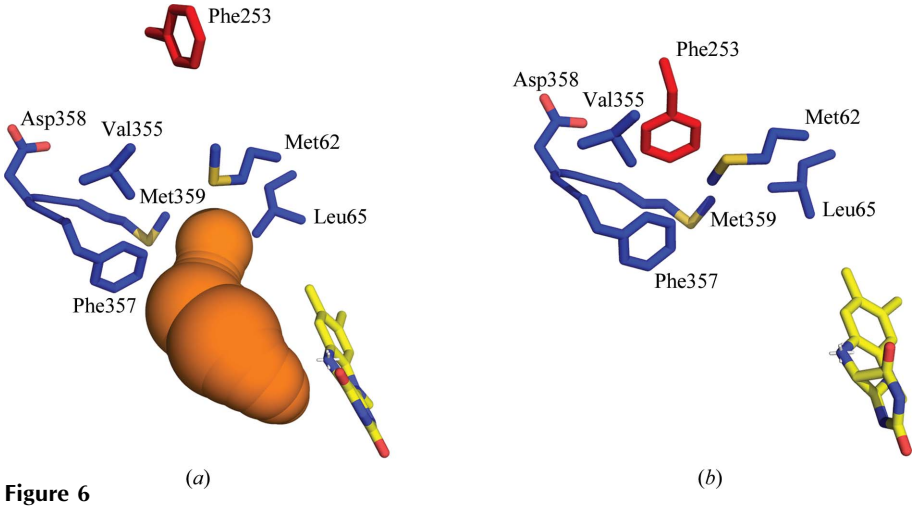

Figure 6
CAVER (Chovancova *et al.*, 2012) analysis of tunnels from the active site to the enzyme surface. (*a*) Choline oxidase in complex with glycine betaine; (*b*) choline oxidase in complex with DMSO. The hydrophobic cluster (Met62, Leu65, Val355, Phe357 and Met359) and the residue Asp358 are shown as blue sticks, FAD is shown as yellow sticks and the side chain of Phe253 of the other subunit is shown as red sticks. The tunnel with the entrance regulated by the side chains of the hydrophobic cluster Met62, Leu65, Val355, Phe357 and Met359 is colored orange in (*a*).

the importance of hydrophobic interactions between the methyls and active-site residues in choline oxidase (Gadda *et al.*, 2004). This is in agreement with Trp61, Tyr465 and Trp331 forming hydrophobic interactions with the trimethylammonium moiety of glycine betaine, as observed in the structure of the enzyme–glycine betaine complex. It is noteworthy that the carboxylate of acetate in the previously published crystal structure of the S101A enzyme (Finnegan, Yuan *et al.*, 2010) has a different orientation from the carboxylate in glycine betaine, further consistent with the importance of the trimethylammonium moiety in ligand binding.

The C^{α} atom of glycine betaine, which corresponds to the C^{β} atom of choline before its oxidation by the enzyme, is close to both His351 and Val464 (Fig. 3). A mechanistic investigation of His351 through site-directed mutagenesis showed that this residue is important for substrate binding and positioning and contributes to the stabilization of the transition state for the hydride-transfer reaction catalyzed by the enzyme (Rungsrisuriyachai & Gadda, 2008). A mechanistic study on Val464 mutants replaced with threonine or alanine showed that the size and hydrophobic character of this residue are important for the localization of O_2 close to the FAD C(4a) atom, allowing the reoxidation of the reduced flavin in turnover (Finnegan, Agniswamy *et al.*, 2010).

The two structures of choline oxidase in complex with glycine betaine and DMSO highlight distinct conformations of the loop of residues 250–255, which is located at the poles of the dimer interface close to the proposed site of access to the active site of the other subunit delimited by the hydrophobic cluster Met62, Leu65, Val355, Phe357 and Met359. In the crystal structure of the V464A enzyme without any bound ligand, loop 250–255 is present in both the open conformation in one subunit and in the closed conformation in the other subunit. This indicates the variability of this loop in the different structures of the enzyme. The closed conformation results in a constricted access of the tunnel entrance delimited by the hydrophobic cluster to access the active site. Thus, the active site is secluded from the bulk solvent when loop is in the closed conformation, which is probably required for the hydride tunneling and for the reactivity of the reduced flavin cofactor with oxygen. Interestingly, this loop assumes an open conformation when the product is bound in the active site. In the case of the previously published crystal structure of wild-type enzyme with DMSO loop 250–255 is present in a closed conformation, whereas in the crystal structure of choline oxidase with the natural product glycine betaine the same loop assumes an open conformation (Fig. 5). We hypothesize that loop 250–255 swings between the open and closed conformations in the ligand-free form of the enzyme and is then stabilized in the closed conformation upon substrate binding to provide an optimal environment for the hydride tunneling and for oxygen reactivity. It is possible that the water involved in the reaction is already present in the active site when choline is bound with the closed loop. The water molecule would become reactive for hydration only upon formation of the aldehyde intermediate. Alternatively, the open conformation of loop 250–255 observed in the crystal structure of the enzyme in complex with glycine betaine could be triggered by the formation of the product in the active site and play a role in product release.

Software tools that compute tunnels in structures of proteins can give important insights into substrate access to the active site and the residues located around bottlenecks of tunnels (Gora *et al.*, 2013). The predicted tunnel in the structure of choline oxidase in complex with glycine betaine through the entrance delimited by the side chains of the hydrophobic cluster Met62, Leu65, Val355, Phe357 and Met359 is likely to be utilized by choline and glycine betaine to enter and leave the active-site cavity (Fig. 6). The side chain of Asp358 is located near the entrance of the tunnel, consistent with a role of electrostatics in guiding positively charged choline into the active site, as described in a previous computational study of choline oxidase (Xin *et al.*, 2009). In the case of the enzyme complex with DMSO, no tunnel was predicted as a consequence of the closed conformation of loop 250–255 and the rotated side chain of Phe253 (Fig. 6). In the free enzyme devoid of ligands, exemplified by the structure of the V464A enzyme, which is almost identical to that of the wild-type enzyme, both open and closed conformations of loop 250–255 are present in the two subunits, with the tunnel entrance open or constricted, respectively (data not shown).

5. Conclusions

The crystal structure of choline oxidase in complex with the reaction product glycine betaine was solved to a resolution of 1.95 Å. This crystal structure is the first structure to be reported for choline oxidase with the physiological product bound and the second of a flavoenzyme of the GMC superfamily with a natural ligand in the active site. The fact that choline oxidase has been extensively characterized kinetically allows the comparison of the new structural data for glycine betaine in the active site with the kinetic data obtained by previous studies. The residues that were concluded to be important for catalysis by kinetic studies are confirmed in their role by their interactions with glycine betaine observed in the present crystal structure. Moreover, the present study suggests the direction of further studies on choline oxidase, such as investigation of His466 as the catalytic base in the active site of the enzyme. The prediction of tunnels highlights the role of the hydrophobic cluster Met62, Leu65, Val355, Phe357 and Met359 as the bottleneck of the tunnel leading to the active site. Further studies will be undertaken using site-directed mutagenesis of the side chains of the hydrophobic cluster Met62, Leu65, Val355, Phe357 and Met359.

One main difference is described between the crystal structures of choline oxidase with DMSO (Quaye *et al.*, 2008) and with glycine betaine. The shift of loop 250–255 and in particular the highly flexible side chain of Phe253 define an open and a closed conformation that are consistent with a gating mechanism to control access to the active site through a pore delimited by the hydrophobic residues Met62, Leu65, Val355, Phe357 and Met359. This study sets the stage for future studies of site-directed mutagenesis of Phe253 to

investigate its role in controlling substrate access to the active site. The different conformations of loop 250–255, especially of Phe253, which covers the active site of the other subunit, suggest that an important role is played by the dimeric state of the enzyme in controlling substrate access.

X-ray data were collected on the Southeast Regional Collaborative Access Team (SER-CAT) beamline 22-ID at the Advanced Photon Source, Argonne National Laboratory. Supporting institutions may be found at http://www.ser-cat.org/members.html. Use of the Advanced Photon Source was supported by the US Department of Energy, Office of Science, Office of Basic Energy Sciences under Contract No. W-31-109-Eng-38. We thank Elvira Romero for purifying the enzyme, Johnson Agniswamy for mounting the protein crystals and for data collection, and Robert Harrison for insightful discussions. This work was supported in part by Grant MCB-1121695 from the NSF (GG).

References

Bannwarth, M., Bastian, S., Heckmann-Pohl, D., Giffhorn, F. & Schulz, G. E. (2004). *Biochemistry*, **43**, 11683–11690.

Bannwarth, M., Heckmann-Pohl, D., Bastian, S., Giffhorn, F. & Schulz, G. E. (2006). *Biochemistry*, **45**, 6587–6595.

Baron, R., Riley, C., Chenprakhon, P., Thotsaporn, K., Winter, R. T., Alfieri, A., Forneris, F., van Berkel, W. J., Chaiyen, P., Fraaije, M. W., Mattevi, A. & McCammon, J. A. (2009). *Proc. Natl Acad. Sci. USA*, **106**, 10603–10608.

Bremer, E. & Kramer, R. (2000). *Bacterial Stress Responses*, edited by G. Stortz & R. Hengge-Aronis, pp. 79–97. Washington: ASM Press.

Cavener, D. R. (1992). *J. Mol. Biol.* **223**, 811–814.

Chen, X., Wolfgang, D. E. & Sampson, N. S. (2000). *Biochemistry*, **39**, 13383–13389.

Chovancova, E., Pavelka, A., Benes, P., Strnad, O., Brezovsky, J., Kozlikova, B., Gora, A., Sustr, V., Klvana, M., Medek, P., Biedermannova, L., Sochor, J. & Damborsky, J. (2012). *PLoS Comput. Biol.* **8**, e1002708.

Dixon, D. A., Lindner, D. L., Branchaud, B. & Lipscomb, W. N. (1979). *Biochemistry*, **18**, 5770–5775.

Emsley, P. & Cowtan, K. (2004). *Acta Cryst.* D**60**, 2126–2132.

Fan, F. & Gadda, G. (2005*a*). *J. Am. Chem. Soc.* **127**, 2067–2074.

Fan, F. & Gadda, G. (2005*b*). *J. Am. Chem. Soc.* **127**, 17954–17961.

Fan, F. & Gadda, G. (2007). *Biochemistry*, **46**, 6402–6408.

Fan, F., Germann, M. W. & Gadda, G. (2006). *Biochemistry*, **45**, 1979–1986.

Fan, F., Ghanem, M. & Gadda, G. (2004). *Arch. Biochem. Biophys.* **421**, 149–158.

Finnegan, S., Agniswamy, J., Weber, I. T. & Gadda, G. (2010). *Biochemistry*, **49**, 2952–2961.

Finnegan, S. & Gadda, G. (2008). *Biochemistry*, **47**, 13850–13861.

Finnegan, S., Yuan, H., Wang, Y.-F., Orville, A. M., Weber, I. T. & Gadda, G. (2010). *Arch. Biochem. Biophys.* **501**, 207–213.

Fu, G., Yuan, H., Li, C., Lu, C.-D., Gadda, G. & Weber, I. T. (2010). *Biochemistry*, **49**, 8535–8545.

Gadda, G. (2003). *Biochim. Biophys. Acta*, **1646**, 112–118.

Gadda, G. (2012*a*). *Biochemistry*, **51**, 2662–2669.

Gadda, G. (2012*b*). *Handbook of Flavoproteins*, edited by R. Hille, S. Miller & B. Palfey, pp. 155–176. Berlin: Walter de Gruyter.

Gadda, G., Fan, F. & Hoang, J. V. (2006). *Arch. Biochem. Biophys.* **451**, 182–187.

Gadda, G., Powell, N. L. & Menon, P. (2004). *Arch. Biochem. Biophys.* **430**, 264–273.

Ghanem, M. & Gadda, G. (2005). *Biochemistry*, **44**, 893–904.

Giri, J. (2011). *Plant Signal. Behav.* **6**, 1746–1751.

Gora, A., Brezovsky, J. & Damborsky, J. (2013). *Chem. Rev.* **113**, 5871–5923.

Hallberg, B. M., Leitner, C., Haltrich, D. & Divne, C. (2004). *J. Mol. Biol.* **341**, 781–796.

Hernández-Ortega, A., Borrelli, K., Ferreira, P., Medina, M., Martínez, A. T. & Guallar, V. (2011). *Biochem. J.* **436**, 341–350.

Krissinel, E. & Henrick, K. (2004). *Acta Cryst.* D**60**, 2256–2268.

Kujawa, M., Ebner, H., Leitner, C., Hallberg, B. M., Prongjit, M., Sucharitakul, J., Ludwig, R., Rudsander, U., Peterbauer, C., Chaiyen, P., Haltrich, D. & Divne, C. (2006). *J. Biol. Chem.* **281**, 35104–35115.

Lambou, K., Pennati, A., Valsecchi, I., Tada, R., Sherman, S., Sato, H., Beau, R., Gadda, G. & Latgé, J.-P. (2013). *Eukaryot. Cell*, **12**, 853–863.

McCoy, A. J., Grosse-Kunstleve, R. W., Storoni, L. C. & Read, R. J. (2005). *Acta Cryst.* D**61**, 458–464.

McNicholas, S., Potterton, E., Wilson, K. S. & Noble, M. E. M. (2011). *Acta Cryst.* D**67**, 386–394.

Murshudov, G. N., Skubák, P., Lebedev, A. A., Pannu, N. S., Steiner, R. A., Nicholls, R. A., Winn, M. D., Long, F. & Vagin, A. A. (2011). *Acta Cryst.* D**67**, 355–367.

Orville, A. M., Lountos, G. T., Finnegan, S., Gadda, G. & Prabhakar, R. (2009). *Biochemistry*, **48**, 720–728.

Otwinowski, Z. & Minor, W. (1997). *Methods Enzymol.* **276**, 307–326.

Quaye, O., Cowins, S. & Gadda, G. (2009). *J. Biol. Chem.* **284**, 16990–16997.

Quaye, O. & Gadda, G. (2009). *Arch. Biochem. Biophys.* **489**, 10–14.

Quaye, O., Lountos, G. T., Fan, F., Orville, A. M. & Gadda, G. (2008). *Biochemistry*, **47**, 243–256.

Quaye, O., Nguyen, T., Gannavaram, S., Pennati, A. & Gadda, G. (2010). *Arch. Biochem. Biophys.* **499**, 1–5.

Rungsrisuriyachai, K. & Gadda, G. (2008). *Biochemistry*, **47**, 6762–6769.

Rungsrisuriyachai, K. & Gadda, G. (2010). *Biochemistry*, **49**, 2483–2490.

Sakamoto, A. & Murata, N. (2000). *J. Exp. Bot.* **51**, 81–88.

Salvi, F. & Gadda, G. (2013). *Arch. Biochem. Biophys.* **537**, 243–252

Sampson, N. S., Kass, I. J. & Ghoshroy, K. B. (1998). *Biochemistry*, **37**, 5770–5778.

Shimomura, T., Itoh, T., Sumiya, T., Mizukami, F. & Ono, M. (2009). *Talanta*, **78**, 217–220.

Spadiut, O., Tan, T.-C., Pisanelli, I., Haltrich, D. & Divne, C. (2010). *FEBS J.* **277**, 2892–2909.

Winn, M. D. *et al.* (2011). *Acta Cryst.* D**67**, 235–242.

Wongnate, T., Sucharitakul, J. & Chaiyen, P. (2011). *Chembiochem*, **12**, 2577–2586.

Xin, Y., Gadda, G. & Hamelberg, D. (2009). *Biochemistry*, **48**, 9599–9605.

Yuan, H. & Gadda, G. (2011). *Biochemistry*, **50**, 770–779.

Yue, Q. K., Kass, I. J., Sampson, N. S. & Vrielink, A. (1999). *Biochemistry*, **38**, 4277–4286.